FULL PAPERS

Magnetic Resonance in Medicine 44:387–394 (2000)

Single-Shot, Three-Dimensional "Non-echo" Localization Method for In Vivo NMR Spectroscopy

In-Young Choi, Ivan Tkáč, and Rolf Gruetter*

Metabolite signals with short T_1 or T_2 are difficult to localize with full sensitivity. This limitation was overcome with the development and implementation of a single-shot, complete three-dimensional "non-echo" localization method with reduced sensitivity to spatial B_1 variation, which is suitable for measuring signals with very short T_1 or T_2, e.g., the ^{13}C NMR signals of glycogen. The proposed method is based on a T_1-optimized outer volume suppression scheme using pulses of the hyperbolic secant type applied at different power levels, which is robust over a fivefold range of T_1. Strong lipid, muscle glycogen, and glucose signals originating outside the rat brain were suppressed. Signals of glycogen, aspartate, glutathione, GABA *C*4, N-acetyl aspartate as well as the *C*3 and *C*4 signals of glutamate and glutamine with resolved homonuclear ^{13}C-^{13}C coupling were fully resolved in vivo at 9.4 Tesla using higher-order shimming. The method can be extended to other nuclei and to localized MRS of humans. Magn Reson Med 44: 387–394, 2000. © 2000 Wiley-Liss, Inc.

Key words: MRS; localization; in vivo; glycogen; glutathione; brain

In vivo NMR spectroscopy (MRS) allows reliable non-invasive studies of metabolism and is a notable modality in biochemistry and physiology (1). Using in vivo MRS, metabolites that play significant roles in intermediary metabolism can be monitored and quantified to determine the rates of metabolic reactions taking place in vivo, thereby leading to a better understanding of metabolism (2). However, the precise localization of fast relaxing signals in vivo, such as those from glycogen (3), an important energy reserve, has been challenging.

Spatial localization is desirable to eliminate signal contamination from outside of the volume of interest (VOI) and is essential for the reliable quantification of metabolite concentrations in vivo. However, the demands placed on a localization method are especially challenging for ^{13}C NMR due to the large chemical shift displacement error and the low sensitivity. In addition, a surface coil used often as a transceiver to increase the sensitivity results in potential signal loss due to the spatially inhomogeneous RF field, B_1. Signal reductions due to the B_1 inhomogeneity can be minimized for ^{13}C NMR using three-dimensional localization based on ISIS using adiabatic RF pulses (4). Moreover, ^{1}H-localized ^{13}C NMR using polarization transfer provides additional signal to noise ratio (SNR) improvements with more precise voxel definition (5). To minimize the signals from non-cerebral tissue in brain studies and to reduce a large chemical shift displacement error, more efforts on three-dimensional localization have been added (6). Alternatively, chemical shift imaging (CSI) can be used for localization of signals with short T_2 (7). However, limited sampling in *k*-space can be used only due to the low sensitivity of ^{13}C NMR, which results in truncation artifacts and contamination of spectra by the intense superficial lipid signals (8). All of the above described localization methods suffer from signal loss when used for the localization of weak signals with very short T_1 and/or T_2, such as cerebral glycogen (~5 μmol/g, T_1 = ~0.3 sec, T_2 = ~6 msec). In order to detect such small signals with very short T_1 or T_2 relaxation, signal attenuation during RF irradiation and/or echo time delays must be minimized. Thus, all localization methods used to date for the ^{13}C NMR detection of glycogen have been restricted to one or two dimensions using a B_0 spoiler (9) or 1D-ISIS (10).

The three most frequently used localization methods are STEAM (stimulated echo acquisition mode) (11), PRESS (point resolved spectroscopy) (12) or ISIS (image-selected in vivo spectroscopy) (13). When using STEAM, metabolites with short transverse relaxation time (T_2) can be detected, since very short echo times on the order of 1 msec can be achieved (14). However, STEAM can detect at most half of the potential signal from the voxel, and signal intensity can be further reduced due to T_2 decay when T_2 is comparable to the echo time, TE. Furthermore, incorporation of B_1-insensitive RF pulses has not been achieved to date. PRESS, on the other hand, uses the full z-magnetization (M_0), resulting in an up to twofold signal intensity gain compared to STEAM and can be combined with adiabatic 180° pulses that minimize the effects of the B_1 inhomogeneity (15). However, PRESS requires longer TE, thereby limiting its use for the detection of compounds with very short T_2. Unlike STEAM and PRESS, ISIS does not require the generation of an echo. In addition, adiabatic pulses are easily incorporated into ISIS (4,16,17). However, ISIS relies on inverting the magnetization in the region of interest, which can result in signal loss due to T_1 relaxation and imperfect slice profile for metabolites with short relaxation times (16). Moreover, ISIS requires a signal addition/subtraction scheme over multiple data acquisitions to select a VOI, which may increase the possibility of incomplete signal subtraction due to subject motion in vivo. Motion might be problematic for in vivo studies of

Center for Magnetic Resonance Research, Department of Radiology, University of Minnesota Medical School, Minneapolis, Minnesota.

Grant sponsor: National Institutes of Health; Grant numbers: P41RR08079; R01NS38672; R21DK58004; Grant sponsors: Whitaker Foundation; University of Minnesota Graduate School.

*Correspondence to: Rolf Gruetter, Center for Magnetic Resonance Research, 2021 6th Street SE, Minneapolis, MN 55455.
E-mail: gruetter@cmrr.umn.edu

Received 26 January 2000; revised 18 April 2000; accepted 19 April 2000.

intact organs, which cannot be immobilized, such as the liver. Therefore, a single-shot, reasonably B_1-insensitive localization method that does not depend on echo-generation is needed to measure signals with very short T_1 or T_2 in vivo.

Localization based on outer volume suppression (OVS) combines slice-selective saturation pulses to minimize z-magnetization outside the VOI and has been used mainly in conjunction with volume coils with other pulse sequences to enhance localization performance (18,19). However, full three-dimensional localization based on OVS alone has not been reported to date.

The purpose of this study was the development and implementation of a single-shot, inversion recovery based, non-echo (SIRENE) three-dimensional localization method based on OVS with minimal reduction of sensitivity in the VOI for fast relaxing signals. In designing the pulse sequence, the localization of signals with a wide range of T_1 or T_2 was considered as well as the minimization of chemical shift displacement error using broadband hyperbolic secant (HS) pulses combined with strong gradients. The performance of the sequence was tested and verified using multi-chamber phantoms. In vivo verification of the localization efficiency was done in the rat brain using two distinct characteristics: (a) natural abundance cerebral lipids in the normal brain are not detectable (4,5,20,21) and (b) post-mortem breakdown of cerebral glycogen and glucose is rapid (22). A preliminary report of this work has appeared (23).

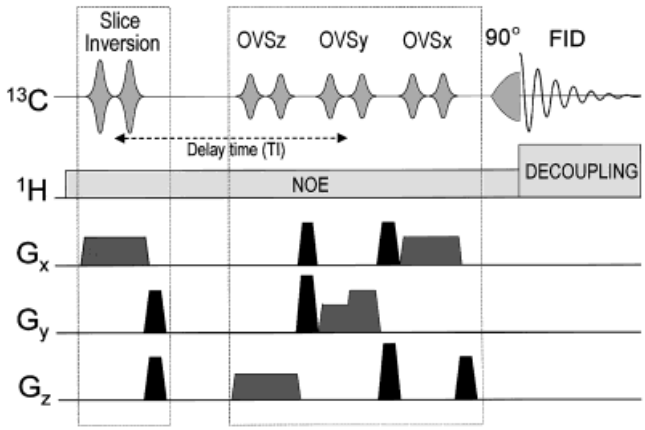

FIG. 1. Pulse sequence diagram for three-dimensional localization based on OVS. Adiabatic pulses (HS8 modulation) were applied to invert the z-magnetization in two x-slices adjacent to VOI. Magnetization in these slices followed an inversion recovery trajectory independent of B_1 and was minimized by adjusting the delay time, TI. Residual magnetization outside of the VOI was further suppressed by using six OVS pulses applied with a nominal 90° flip angle. Slice-selection gradients are shown shaded. The thickness of the upper and lower saturated y-slices was different to adapt to the geometry of the rat head. Transverse magnetization was dephased by spoiling gradients (solid black). An adiabatic half passage (AHP) pulse was used for excitation. Bi-level WALTZ-16 was applied on ^{1}H channel for NOE and decoupling.

MATERIALS AND METHODS

NMR Methods

All experiments were performed on a 9.4 T, 31 cm bore horizontal magnet (Magnex Scientific, UK), interfaced to a INOVA console (Varian, Palo Alto, CA) using an actively shielded gradient coil (Magnex Scientific, UK) with an 11 cm inner diameter, which was capable of switching to 300 mT/m in 500 μsec. A quadrature ^{1}H surface RF coil (14 mm diameter) combined with a linear three-turn ^{13}C coil (12 mm diameter) was built according to Adriany and Gruetter (24). A small sphere (3 mm diameter) containing 99% ^{13}C-enriched formic acid was placed at the center of the ^{13}C linear coil as an external reference. Automated localized shimming using a fully adiabatic version of FASTMAP (25,26) was used to adjust the currents in all first- and second-order shim coils. The field homogeneity resulted in a 18–26 Hz full width at half maximum of the in vivo water signal in a nominal 500 μl volume.

Pulse Sequence

To illustrate the selected features of slice gradient orientations, the following convention is used throughout this paper: z is parallel to B_0, y is parallel to the ^{13}C coil axis ("vertical" axis) and x denotes the orientation perpendicular to the ^{13}C coil axis and perpendicular to B_0 ("horizontal" axis). The pulse sequence (Fig. 1) consisted of three stages. First, slice-selective adiabatic pulses were applied in conjunction with gradients along x to invert the z-magnetization in two x-slices adjacent to the VOI. Since the sensitive volume of the RF coil extends longer along x than along z, B_1 variations and signals were estimated to be strongest in x-slices (e.g. temporal muscle in the rat head). To minimize the z-magnetization in these slices in a B_1-insensitive manner, the magnetization was inverted using adiabatic RF pulses and an inversion recovery delay time (TI) was inserted according to the measured T_1 of the signals of interest.

Second, at the time when the inverted z-magnetization in x-slices was approaching zero, six HS pulses with nominal 90° flip angles and concomitant gradients were applied to minimize the residual z-magnetization in six slices surrounding the VOI in the following order: z, y, and then x. Additionally, an optional alternating 180° pulse with corresponding phase cycling was applied with a concomitant y gradient to select a y-slice containing the voxel to decrease the sensitivity of the localization performance to power settings of the OVS.

All RF pulses used for OVS were of the HS type as described previously (27). The advantages of HS pulses are a B_1-insensitive profile even for a nominal 90° flip angle and broad bandwidths, which minimize chemical shift displacement error. The HS pulse shapes were tailored to meet the specific needs of the in vivo geometry (see below) and the RF power was adjusted to minimize the z-magnetization outside the VOI. Specifically, an adiabatic full-passage (AFP), HS8 pulse (27) with 10 kHz bandwidth and 8 msec pulse duration was used for inversion in x-slices. These pulses achieved inversion at a low peak $\gamma B_1/2\pi$ of 800 Hz. Crusher gradients were applied subsequently to dephase any residual transverse magnetization. Care was taken in the selection of crusher gradients to avoid generation of unwanted coherences. To improve the localization

performance along y, 6 ms long HS pulses were used with a very narrow transition bandwidth (4.6% of the 10kHz bandwidth at a $\gamma B_1/2\pi$ of 800 Hz). 2 msec long HS pulses with a different R-value were used along x and z to minimize pulse duration and to maximize pulse bandwidth (10kHz bandwidth at a $\gamma B_1/2\pi$ of 1300 Hz). The total time required for the OVS part of the sequence was ~160 msec with a TI of 140 msec and 2 msec crusher gradient duration. With the presently used parameters for gradient switching and RF pulses, the minimum possible TI was ~22 msec.

Third, an adiabatic half-passage (AHP) 90° pulse was used for excitation immediately followed by acquisition of the FID. Bi-level WALTZ-16 RF-pulses were applied to the proton channel for generation of a nuclear Overhauser effect (NOE) between excitations and for decoupling during an acquisition time of 90 msec (28).

T_1 Measurements

To optimize the inversion delay (TI in Fig. 1), T_1 values of several compounds were measured using the inversion recovery method. The power of the adiabatic inversion pulse was set to invert the z-magnetization in the entire sensitive volume of the ^{13}C coil and the repetition time (TR) was at least five times longer than the estimated T_1. T_1 was determined from a three-parameter exponential curve fit and the time required to minimize the z-magnetization "inversion null" was calculated and experimentally confirmed.

Phantom Study

To test the localization efficiency, three different two-compartment phantoms were prepared by placing a smaller cylindrical tube (diameter of 1.4 cm) inside a larger cylindrical tube (diameter of 2.7 cm) with length of 10 cm: (a) 250 mM glutamine (inner compartment) and 2 M acetate (outer compartment); (b) 100 mM *myo*-inositol (inner compartment) and 300 mM oyster glycogen (outer compartment) solution; and (c) 100 mM glucose (inner compartment) and 400 mM oyster glycogen (outer compartment) solution. Two different compounds (e.g., acetate and glycogen) were placed into the outer compartments of these three phantoms in order to test the localization performance of the sequence on signals with a wide range of relaxation times. To imitate various in vivo geometries, (e.g., the muscles on top of the brain being thinner than the temporal muscles) two different phantom geometries were used: To test the sensitivity of the OVS performance on the thickness of the y-slice, the position of the inner cylinder relative to the outer cylinder was varied from 1.8 mm to 3.4 mm.

Animal Preparation

The study was approved by the Institutional Animal Care and Use Committee (IACUC) and followed the guidelines for the care and use of laboratory animals at the University of Minnesota. α-chloralose anesthetized male Sprague-Dawley rats (245 ± 12 g, n = 5) were intubated and ventilated with a pressure-driven ventilator (Kent, Litchfield, CT) with a 60:40 mixture of O_2 and N_2O gases.

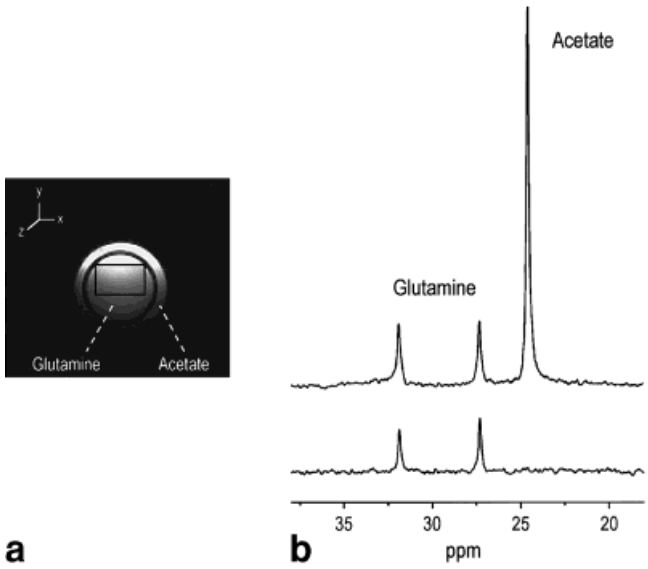

FIG. 2. Validation of three-dimensional localization efficiency on signals with long T_1. **a:** ^1H image of a coaxial two-compartment phantom containing 2 M natural abundance acetate (outer compartment) and 250 mM L-glutamine (inner compartment) acquired in the xy-plane using a FLASH sequence (TR = 10 msec, TE = 5 msec). The selected VOI is shown as a rectangle in the image. **b:** The sixfold stronger acetate signal from outside the VOI (top trace) was completely suppressed into the noise level when localization was applied (bottom trace) (TR = 3 sec, nt = 256, TI = 1.4 sec).

Catheters were inserted in the femoral artery and veins for blood gas analysis, α-chloralose and glucose infusion, and physiological monitoring of blood pressure and heart rate. The animals were then placed in an acrylic holder attached to an insert in the gradient coil. The body temperature of animals was maintained at 37°C with a warm water circulation system using the feedback of a rectal temperature probe (Cole Palmer, Vernon Hills, IL). Physiological parameters were adjusted and maintained within the normal range throughout the experiments. [1-^{13}C] D-glucose (99% enriched, 20% weight/volume solution, Isotec Inc., Miamisburg, OH) was infused into the femoral vein according to a previously described protocol (22).

RESULTS

Phantom Experiments

Three two-compartment phantoms were used to test the localization performance of the developed pulse sequence (Fig. 1). A criterion for the quality of the localization was complete elimination of signals originating from the outer chambers. The delay time (TI) was based on T_1 measurements. The VOI (~500 μl nominal volume) was placed in the inner cylinder (Fig. 2a). The adiabatic HS8 pulses inverted the z-magnetization in x-slices with minimized B_1 sensitivity. After the delay TI, the z-magnetization in the x-slices approached zero. Because of the adiabatic inversion pulses, the reduction of the longitudinal magnetization was independent of B_1 but dependent on TI relative to T_1. Magnetization was further reduced by using additional RF pulses with a nominal 90° flip angle whose

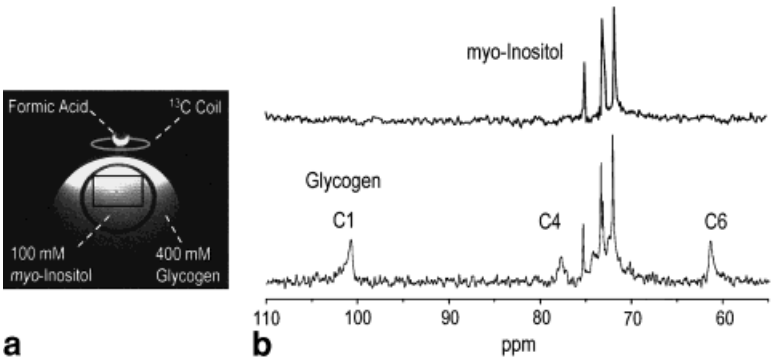

FIG. 3. Localization efficiency for a signal with short T_1 (glycogen). **a:** ^{1}H image of the two-compartment phantom, 400 mM oyster glycogen (outer compartment, T_1 = ~0.3 sec) and 100 mM *myo*-inositol (inner compartment), mimicking in vivo geometry of the rat brain acquired using a FLASH sequence. **b:** To demonstrate of the localization efficiency for glycogen signals, ^{13}C spectra were acquired with localization (top trace) and without localization (bottom trace). The glycogen signals in the localized spectrum were suppressed well into the noise level (TR = 1 sec, nt = 1000, TI = 0.14 sec). The localization reference frequency was set to 100.6 ppm.

power was then optimized to suppress the outer volume signals in z, y, and x-slices completely. The RF power was adjusted for each experiment based on 180° flip angle measurements on an external reference signal (^{13}C formic acid). RF power of all OVS pulses was calibrated based on the ratio between the power requirements for the 180° pulse on the formic acid signal relative to the OVS pulses, which was experimentally determined in phantoms. Localization performance was insensitive to the power setting of the nominal 90° OVS pulses within ± 2 dB.

Figure 2a shows a transverse ^{1}H image of a coaxial two-chamber phantom containing glutamine inside and acetate outside. To demonstrate the performance of the localization, ^{13}C NMR spectra were acquired from this phantom with and without localization (Fig. 2b). The top trace shows the unlocalized spectrum, which includes the signals of glutamine and acetate from both inner and outer compartments. The bottom trace shows the localized spectrum, in which the more than sixfold higher signal of acetate with very long T_1 (T_1 = ~7 sec) from the outer compartment was completely eliminated with minimal reduction of the glutamine signal from inner compartment (TI = 1.4 sec).

A transverse image of a two-compartment phantom mimicking more closely the in vivo geometry (e.g., rat head) was obtained using a FLASH sequence (Fig. 3a). In the unlocalized spectrum, signals from both *myo*-inositol and glycogen were clearly observed (Fig. 3b, bottom trace), whereas in the localized spectrum (Fig. 3b, top trace) the glycogen signals from the outer cylinder were within the noise, thereby illustrating the localization efficiency of the method for oyster glycogen (T_1 = 0.34 ± 0.01 sec, mean ± standard deviation, n = 7). In conjunction with Fig. 2, this demonstrates the performance of the pulse sequence in a wide range of T_1 from ~0.3 to ~7 sec, which is a 20-fold variation, while the TI was varied from 0.14 to 1.4 sec.

^{13}C images were used to demonstrate the localization efficiency of the sequence shown in Fig. 1 (Fig. 4). The ^{13}C images of a phantom containing a 20% weight/volume solution of 99% enriched [1-^{13}C] glucose were acquired with a gradient-echo readout (TR = 965 msec, TE = 2.1 msec, 64 phase encoding steps, number of transients = 128, FOV = 3 × 3 cm^2, slice thickness = 3 mm) following the OVS pulses. Without OVS, this image (Fig. 4a) showed the sensitive volume of the ^{13}C coil. The nominal VOI (8.5 × 6 × 10 mm^3) is indicated by the dotted rectangle in Fig. 4a. Fig. 4b shows that signals from outside the VOI were well suppressed by applying the OVS pulses prior to the image acquisition, indicating a good voxel definition of the localization method. The reference frequency for the VOI selection was set to the *C*1 resonance of β-glucose at 96.8 ppm. The sphere containing the 99% formic acid was thus displaced by ~3 mm due to the chemical shift difference relative to the glucose *C*1 resonance, consistent with the readout gradient of 200 mT/m corresponding to 21.3 kHz/cm and the chemical shift difference of ~70 ppm = 7 kHz.

In Vivo Experiments

A 500 μl VOI was placed in the rat brain on the midline and 1.5 mm posterior to the bregma. The power of the RF pulses was calculated from the pulsewidth needed to invert magnetization of the ^{13}C formic acid signal from the sphere located at the center of the linear ^{13}C coil. Following this measurement, which assesses variability in coil loading, no further RF power adjustment of the six 90° OVS pulses was made. Thus no time was required to optimize OVS. To optimize TI for glycogen, lipids and other amino acids, T_1 measurements were performed us-

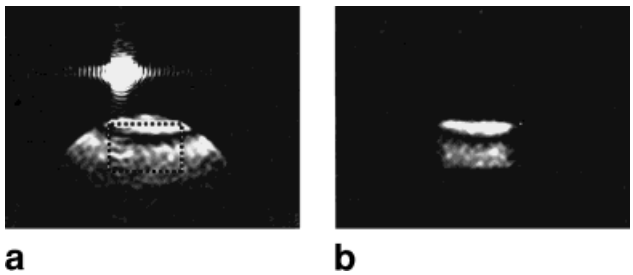

FIG. 4. ^{13}C MRI of the three-dimensional localization efficiency of the sequence in Fig. 1. **a:** ^{13}C image of [1-^{13}C] glucose phantom was acquired using a gradient-echo readout following OVS localization (TE = 2.1 msec, TR = 965 msec, 64 phase encoding steps). The dashed rectangle in the image indicates the location of the selected voxel. The bright spot was from the sphere containing 99% enriched ^{13}C formic acid at the center of ^{13}C coil, consistent with the chemical shift displacement in the readout direction (x-axis). The ^{13}C-image acquisition following OVS (**b**) shows excellent correspondence to the selected voxel shown in the unlocalized image (**a**). The dark band within the selected volume corresponds to the area of inverted z-magnetization due to the use of surface coil and Gaussian RF pulses used for excitation.

Table 1
In Vivo T_1 of ^{13}C NMR Resonances

Metabolites	^{13}C chemical shift (ppm)	T_1 (sec)
Glycogen C1	100.64	0.33 ± 0.03[b]
Glucose C1β	96.80	1.48 ± 0.13[b]
Lipid	30.50	0.59 ± 0.04[b]
Glutamate C4	34.27[a]	1.27 ± 0.05
Glutamine C4	31.66	1.22 ± 0.06
Glutamate C3	27.74	1.17 ± 0.12
Glutamine C3	27.08	1.23 ± 0.23
Aspartate C3	37.36	1.33 ± 0.11
N-acetyl-aspartate C3	40.45	1.07 ± 0.18
GABA C2	35.12	1.28 ± 0.35

*T_1 of extracerebral lipid and of metabolite signals from the rat brain in vivo at 9.4 T. T_1 values were obtained by a non-linear three-parameter exponential curve fit.
[a]^{13}C chemical shifts were referenced relative to the Glutamate *C*4 peak based on Barany et al. (39) except for the glycogen *C*1 peak, which was referenced to the β-glucose *C*1 peak (96.8 ppm).
[b]T_1 values were estimated from five measurements (mean ± standard deviation) and all other T_1 values were from four measurements in three animals.

ing the inversion recovery method. The T_1 of glycogen *C*1 in vivo was 0.33 ± 0.03 sec and that of lipids was 0.59 ± 0.04 sec. The T_1 of several metabolites in vivo including glutamate *C*4, GABA C2, and lipid are shown in Table 1. Examples of the measured inversion recovery time courses are shown in Fig. 5.

Figure 6 shows an in vivo localized ^{13}C NMR spectrum acquired with the sequence and a corresponding transverse ^{1}H image of the rat brain. The localization method completely eliminated the extraneous methylene lipid signals that resonate at ~30.5 ppm (T_1 = ~0.6 sec, Table 1) confirming the effectiveness of the localization. A well-defined volume within the brain and localized higher-order shimming resulted in an excellent spectral resolution demonstrated by the resolved homonuclear ^{13}C-^{13}C coupled spin systems (J_{CC} = 34 Hz) of the glutamate *C*4 and *C*3 resonances. In addition, homonuclear coupling was detected in the glutamine *C*4 and *C*3, the aspartate *C*3 and the GABA *C*3 resonances. All glutamine resonances and the glutathione resonance at 32.16 ppm were completely resolved from glutamate at 9.4 Tesla. Additionally, the GABA *C*4 resonance at 40.35 ppm was discernible from the resonance of NAA *C*3. Such a level of in vivo specificity has not been reported to date. The sequence also provided excellent sensitivity, as illustrated by the detection of the NAA and lactate methyl resonances using NOE enhancement.

To further confirm the localization performance, we observed the rapid post-mortem degradation of brain glycogen compared to muscle glycogen. The localized glycogen and glucose signals reduced to the noise level within a few minutes while the unlocalized signal persisted for several hours, as described elsewhere (22). Specifically, the simultaneous detection of muscle glycogen and glucose signals in spectra from the post-mortem rat head and their elimination upon localization (Fig. 2 in Ref. 22) further illustrated the ability of the sequence to simultaneously provide accurate localization of signals with widely different T_1 as illustrated for glucose and glycogen in Table 1.

DISCUSSION

In this paper, we report the development and implementation of a single-shot three-dimensional localization method for in vivo ^{13}C NMR spectroscopy based on outer volume suppression (OVS). To minimize sensitivity to B_1 variations, typically encountered when using surface coils, the OVS method used inversion recovery in x-slices, having the largest B_1 inhomogeneity and most stringent requirements for suppressing signal from outside the VOI. Excellent performance of the localization of signals with a relatively short T_1, such as glycogen (T_1 = ~0.3 sec, Table 1) and extraneous lipid resonances (T_1 = ~0.6 sec, Table 1), became possible for the first time as shown in (22) and in Fig. 6. The T_1 of glycogen measured in the rat brain (Table 1) was comparable to the T_1 of oyster glycogen (0.34 ± 0.01 sec) at 9.4 T and similar to the T_1 of oyster and liver glycogen at 8.4 T (29). These results are in agreement with a recent study that showed the T_1 of glycogen was independent of molecule size, temperature, and possibly structure (30).

Although localization of signals with a short T_1 was emphasized in the current implementation, we demonstrated accurate localization of signals with longer T_1. Since in vivo T_1 values varied between 0.3 sec (glycogen *C*1) and 1.5 sec (glucose *C*1), adjustments of the delay TI in the pulse sequence (Fig. 1) was minimal. Evidence that accurate localization is simultaneously possible for signals covering the range of typical in vivo T_1 (Table 1) was provided by the simultaneous elimination of both muscle

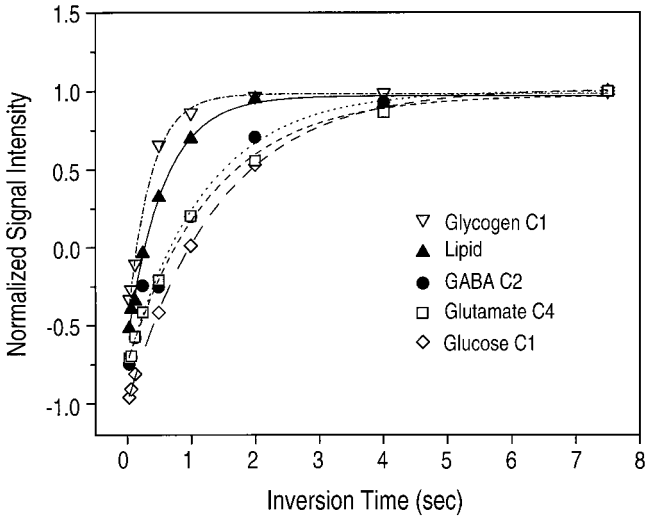

FIG. 5. Inversion recovery trajectories of in vivo signals at 9.4 Tesla. The T_1 of glycogen *C*1 and other metabolites were measured in vivo from a rat head using the inversion recovery method (delay between excitations = 7.5 sec; number of transients was 40 for glycogen and glucose, and 80 for lipid, GABA, and glutamate). The lines are the best three-parameter fit to the corresponding data. The open-triangles, the filled-triangles, filled circles, open squares, and open diamonds indicate the normalized intensity of in vivo cerebral glycogen *C*1 (100.64 ppm), lipid (30.50 ppm), GABA *C*2 (35.12 ppm), glutamate *C*4 (34.27 ppm), and glucose *C*1 (96.80 ppm) signals, respectively. More T_1 values averaged from several studies are listed in Table 1. For these T_1 measurements and those in Table 1, the nominal volume was increased threefold.

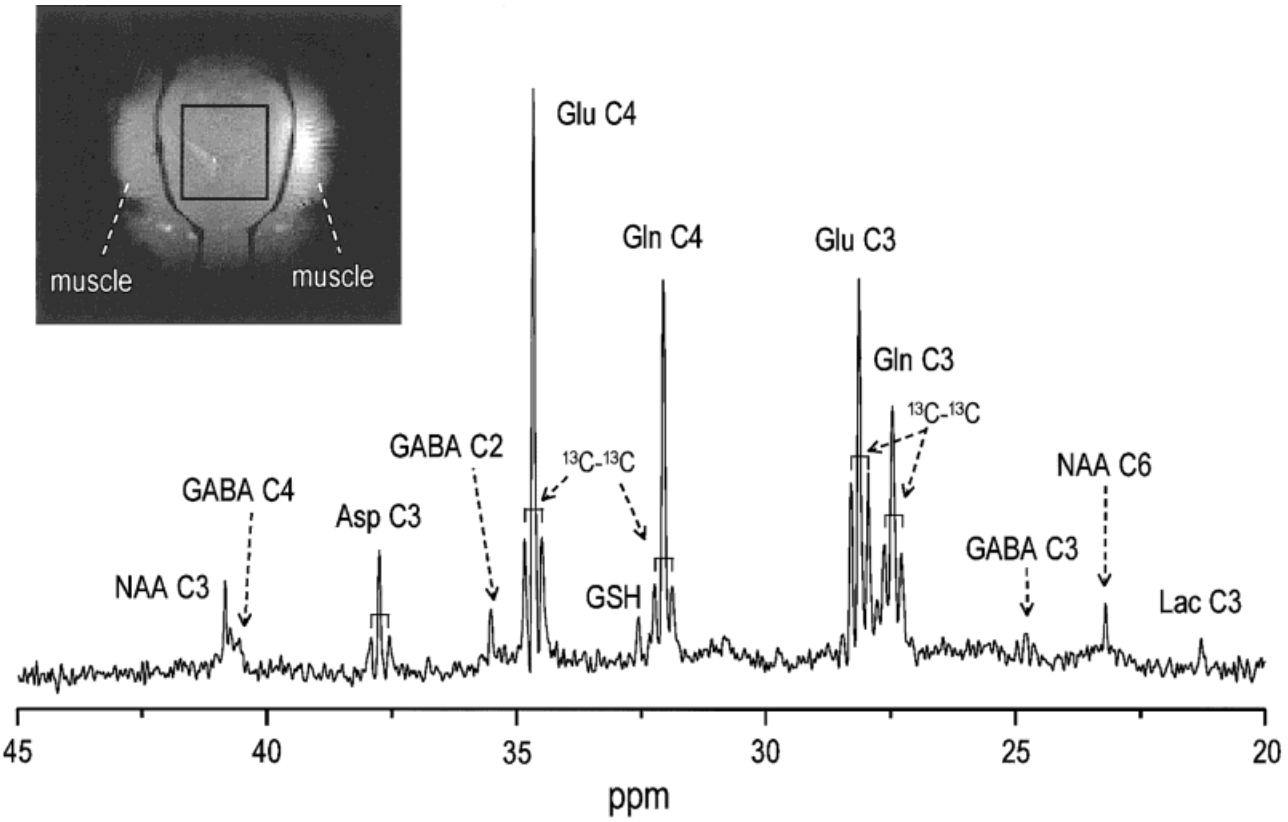

FIG. 6. 3D-localized in vivo ^{13}C NMR spectrum of the rat brain using the single-shot method shown in Fig. 1. The spectrum was acquired in 38 min from the rat brain (TR = 1.5 sec, TI = 0.2 sec) 3.5 hr after starting a 99%-enriched [1-^{13}C] D-glucose infusion from a nominal 500 μl volume. Resonances were identified based on previously reported chemical shifts (40). Homonuclear ^{13}C -^{13}C coupling was observed due to label scrambling in the TCA cycle (20) in glutamate *C*3 and *C*4, glutamine *C*3 and *C*4, aspartate *C*3, and GABA *C*3. In addition, the signal of GABA *C*4 was resolved from that of NAA *C*3 and glutathione (GSH) labeling was detected. The spectrum is shown with 3 Hz Gaussian resolution enhancement applied prior to zero-filling and fast Fourier transformation (FFT). No baseline correction was applied. The inset shows the transverse ^{1}H image placed 1 mm superior (along y) to the center of the VOI. The rectangle indicates the dimension of the nominal VOI (8.5 × 6 × 10 mm^3).

glucose and glycogen signals in the post-mortem rat brain for a given TI (22). Thus, the proposed method enabled simultaneous detection of in vivo signals with both short T_1 and long T_1 as well as short and long T_2. Most resonances from small molecules in vivo (e.g., neurotransmitters and amino acids) appear to have similar T_1 values to that of glucose (Table 1 and Fig. 5), which provides evidence for reliable and well-defined localization for most signals detected in Fig. 6.

Minimizing the chemical shift displacement error is of critical importance for direct-detected in vivo ^{13}C NMR spectroscopy. In our implementation at 9.4 T, the chemical shift difference of 70 ppm (between the glucose *C*1 and glutamate *C*3 resonances) was at most 2.7 mm when using 245 mT/m gradients. We used broadband hyperbolic secant pulses of the HS8 type (27), which provided a 10 kHz bandwidth and achieved full inversion at an RF power corresponding to $\gamma B_1/2\pi$ = 800 Hz. Likewise, the 6 msec and 2 msec long HS pulses produced a nominal 90° flip angle at a $\gamma B_1/2\pi$ of 800 Hz and 1300 Hz, respectively. Therefore, we conclude that the demands on peak RF power must be considered very modest for a small surface coil such as the one used in this study (12 mm diameter). When larger RF coils and weaker gradients are used, the chemical displacement error is expected to be more prominent. However, the method will still provide accurate three-dimensional localization for glycogen and glucose *C*1 resonances. For example, considering at 1.5 T the chemical shift difference between glucose *C*1 and glycogen *C*1 (~7 ppm, i.e. ~110 Hz), HS pulses with 5 kHz bandwidth (a peak $\gamma B_1/2\pi$ of 400 Hz) and 10 mT/m gradients (corresponding to ~1 kHz/cm at the ^{13}C frequency) result in a chemical displacement error of only 2.2% of the voxel dimension, which increases to 22% for a 70 ppm chemical shift range. Such small displacement errors are well within the tolerance for in vivo human applications and point to the potential simultaneous localized detection of the glutamate *C*4 and glucose *C*1 resonance at 1.5 Tesla. In this example, it should be stressed that the limiting factor is the assumed available gradient strength. A 3 Tesla system, for example, with 20 mT/m gradient strength and a peak $\gamma B_1/2\pi$ of 1 kHz (10 kHz bandwidth) results in identical chemical shift displacement errors.

Since the localization part of the sequence does not affect magnetization inside the VOI, the proposed localization method can be combined with low flip angle exci-

tation and short TR, provided the TI is adjusted accordingly, which increases SNR per unit time. The observed insensitivity to spatial B_1 variations and low peak RF power requirements of the OVS pulses implies that the method can also be applied when volume coils are used for RF transmission with minimal RF power adjustments. However, the specific absorption rate (SAR) will be increased and the SNR decreased when detecting with a volume coil. In addition, larger outer volume signals need to be suppressed.

For nuclei where the signals that need to be suppressed are not too large and T_1 or T_2 are similar to the range encountered in this study, we expect that the proposed scheme will be equally applicable, such as localized MRS of ^{15}N and ^{31}P and possibly ^{23}Na as well as CSI of ^{1}H (31), or when using ^{1}H localization combined with polarization transfer to ^{13}C (5,20,32).

To our knowledge, this is the first study to report the acquisition of fully 3D-localized, direct detected ^{13}C NMR signals of the rat brain in vivo. Most studies of the rat brain have been hampered by a requirement to subtract a baseline spectrum containing the natural abundance lipid signals (33). Thus spectra are more prone to small variations in system stability and motions of the animal. Furthermore, elimination of the acquisition of such a natural abundance reference spectrum naturally increases the SNR and decreases experimental time, leading to a compounded increase in sensitivity. It should be emphasized that although a nominal volume size was specified based on the slice-selection parameters, the effective volume is much smaller due to the spatial characteristic of the RF field of the surface coil. For example, when assuming that the sensitive volume of the RF coil equals a half-sphere of equal diameter, a sensitive volume of a 12 mm diameter ^{13}C coil is approximately 400 μl. Therefore, the VOI reported in this paper represents the dimensions selected by the gradient-based localization and can be considered as nominal. Thus the effective volume size is much smaller and probably corresponds to 250 μl.

In conjunction with higher-order shimming based on FASTMAP, we consistently achieved narrow linewidths on the order of 20 Hz for in vivo water, which allowed the routine detection of ^{13}C-^{13}C isotopomers in glutamate and glutamine *C*3 and *C*4 as well as in aspartate *C*3. This is to our knowledge the first in vivo detection of isotopomer signals in glutamate, glutamine, and aspartate in the animal brain upon infusion of singly labeled glucose. Observation of these multiplets, which reflects label scrambling due to TCA cycle activity (2,34), extends previous in vitro isotopomer analysis (35) to the in vivo case. The demonstrated resolution and information content of spectra such as the one shown in Fig. 6 imply the feasibility of metabolic modeling of data obtained from the rodent brain using models of similar and higher complexity as recently proposed for human brain at 4 Tesla (20). In addition, we were able to directly detect the *C*4 resonance of GABA resolved from the adjacent NAA *C*3 resonance, the multiplet of GABA *C*3, and the ^{13}C glutamate *C*4 resonance of glutathione (GSH Glu *C*4) for the first time in vivo. The GSH Glu *C*4 resonance, present in the brain at a sufficient concentration to be detected in vivo by ^{1}H NMR (36,37), was consistently observed at 32.16 ppm. We also noted a small, but consistent labeling of the lactate *C*3 resonance (Fig. 6). Although direct ^{13}C NMR detection may suffer from reduced sensitivity, the method provides much higher chemical specificity and spectral resolution compared to the indirect ^{1}H NMR detection (38).

To date, no localized three-dimensional spectroscopy of glycogen has been reported in humans. Provided that the FDA guidelines for SAR are enforced, the proposed method should be easily transferable to the studies of human glycogen metabolism. In this context, it should be stressed that peak RF power cannot be considered to be a limiting factor for human applications, since the employed pulses can be tailored to perform at very low peak B_1. The resulting improved three-dimensional definition of the VOI is expected to improve reliability and reproducibility of studies of glycogen metabolism in the human liver, muscle, and heart.

CONCLUSIONS

In this study, a single-shot, inversion recovery based, nonecho (SIRENE) three-dimensional localization method for in vivo spectroscopy was developed. We demonstrated for the first time single-shot, three-dimensional localized ^{13}C NMR spectroscopy in the rat brain in vivo with minimal sensitivity reduction. Improved sensitivity was illustrated by the detection of the *C*4 resonance of GABA resolved from the *C*3 of NAA, the detection of the multiplet of GABA *C*3, and glutathione (GSH) labeling for the first time reported in ^{13}C NMR in vivo. Fully resolved signals of intermediary metabolites including lactate, GABA C2, glutamate and glutamine *C*3,4 isotopomers, and aspartate *C*3 isotopomers were detected. We conclude that the proposed localization method should be applicable for other nuclei such as ^{15}N, ^{23}Na and ^{31}P. Moreover, it can be adapted to human applications for the detection of signals from metabolites of low concentrations with various ranges of T_1 and T_2 values. The combination of complete three-dimensional localization and excellent sensitivity will help further understanding of brain glycogen metabolism in the human brain in vivo.

ACKNOWLEDGMENTS

Supported by U.S. public health service grants from the National Institutes of Health, the Whitaker Foundation (R.G.), and a Grant-in-Aid by the University of Minnesota Graduate School (R.G.). We thank Drs. Hellmut Merkle and Gregor Adriany for technical support. The authors express their gratitude for the support and encouragement of Prof. Kamil Ugurbil and Sang-Pil Lee.

REFERENCES

1. Bachelard H. Landmarks in the application of ^{13}C-magnetic resonance spectroscopy to studies of neuronal/glial relationships. Dev Neurosci 1998;20:277–288.
2. Cerdan S, Kunnecke B, Seelig J. Cerebral metabolism of [1,2-$^{13}C_2$]acetate as detected by in vivo and in vitro ^{13}C NMR. J Biol Chem 1990;265:12916–12926.
3. Shulman RG, Bloch G, Rothman DL. In vivo regulation of muscle glycogen synthase and the control of glycogen synthesis. Proc Natl Acad Sci USA 1995;92:8535–8542.

4. Gruetter R, Rothman DL, Novotny EJ, Shulman RG. Localized ^{13}C NMR spectroscopy of myo-inositol in the human brain in vivo. Magn Reson Med 1992;25:204–210.
5. Gruetter R, Adriany G, Merkle H, Andersen PM. Broadband decoupled, 1H localized ^{13}C MRS of the human brain at 4 Tesla. Magn Reson Med 1996;36:659–664.
6. Watanabe H, Ishihara Y, Okamoto K, Oshio K, Kanamatsu T, Tsukada Y. In vivo 3D localized ^{13}C spectroscopy using modified INEPT and DEPT. J Magn Reson 1998;134:214–222.
7. Brown TR, Kincaid BM, Ugurbil K. NMR chemical shift imaging in three dimensions. Proc Natl Acad Sci USA 1982;79:3523–3526.
8. Hu X, Patel M, Chen W, Ugurbil K. Reduction of truncation artifacts in CSI by extended sampling using variable TR. J Magn Reson A 1995; 106:292–296.
9. Jehenson P, Bloch G. Elimination of surface signals by a surface-spoiling magnetic field gradient. Theoretical optimization and application to human in vivo NMR spectroscopy. J Magn Reson 1991;94:59–72.
10. Rothman DL, Magnusson I, Katz LD, Shulman RG, Shulman GI. Quantitation of hepatic glycogenolysis and gluconeogenesis in fasting humans with ^{13}C NMR. Science 1991;254:573–576.
11. Frahm J, Merboldt KD, Hänicke W. Localized proton spectroscopy using stimulated echoes. J Magn Reson 1987;72:502–508.
12. Bottomley PA. Selective volume method for performing localized NMR spectroscopy, in U.S. patent 4 480 228. 1984: USA.
13. Ordidge RJ, Connelly A, Lohman JAB. Image-selected in vivo spectroscopy (ISIS). A new technique for spatially selective NMR spectroscopy. J Magn Reson 1986;66:283–294.
14. Tkac I, Starcuk Z, Choi I-Y, Gruetter R. In vivo 1H NMR spectroscopy of rat brain at 1 ms echo time. Magn Reson Med 1999;41:649–656.
15. de Graaf RA, Luo Y, Garwood M, Nicolay K. B_1-insensitive, single-shot localization and water suppression. J Magn Reson B 1996;113:35–45.
16. Lawry TJ, Karczmar GS, Weiner MW, Matson GB. Computer simulation of MRS localization techniques: an analysis of ISIS. Magn Reson Med 1989;9:299–314.
17. Luyten PR, Groen JP, Vermeulen JW, den Hollander JA. Experimental approaches to image localized human 31P NMR spectroscopy. Magn Reson Med 1989;11:1–21.
18. Shungu DC, Glickson JD. Sensitivity and localization enhancement in multinuclear in vivo NMR spectroscopy by outer volume presaturation. Magn Reson Med 1993;30:661–671.
19. Chen YJ, Rachamadugu S, Fernandez EJ. Three dimensional outer volume suppression for short echo time in vivo 1H spectroscopic imaging in rat brain. Magn Reson Imaging 1997;15:839–845.
20. Gruetter R, Seaquist E, Kim S-W, Ugurbil K. Localized in vivo ^{13}C NMR of glutamate metabolism. Initial results at 4 Tesla. Dev Neurosci 1998; 20:380–388.
21. Gruetter R, Novotny EJ, Boulware SD, Mason GF, Rothman DL, Prichard JW, Shulman RG. Localized ^{13}C NMR spectroscopy of amino acid labeling from [1-^{13}C] D-glucose in the human brain. J Neurochem 1994;63:1377–1385.
22. Choi I-Y, Tkac I, Ugurbil K, Gruetter R. Noninvasive measurements of [1-^{13}C] glycogen concentrations and metabolism in rat brain in vivo. J Neurochem 1999;73:1300–1308.
23. Choi I-Y, Tkac I, Gruetter R. Single-shot, localized, high-resolution in vivo ^{13}C NMR spectroscopy of rat brain. In: Proceedings of the 7th Annual Meeting of ISMRM, Philadelphia, 1999. p 684.
24. Adriany G, Gruetter R. A half volume coil for efficient proton decoupling in humans at 4 Tesla. J Magn Reson 1997;125:178–184.
25. Gruetter R, Weisdorf SA, Rajanayagan V, Terpstra M, Merkle H, Truwit CL, Garwood M, Nyberg SL, Ugurbil K. Resolution improvements in in vivo ^{1}H NMR spectra with increased magnetic field strength. J Magn Reson 1998;135:260–264.
26. Gruetter R. Automatic, localized in vivo adjustment of all first- and second-order shim coils. Magn Reson Med 1993;29:804–811.
27. Tannus A, Garwood M. Improved performance of frequency-swept pulses using offset-independent adiabaticity. J Magn Reson A 1996; 120:133–137.
28. Shaka AJ, Keeler J, Freeman R. Evaluation of a new broadband decoupling sequence: WALTZ-16. J Magn Reson 1983;53:313–340.
29. Zang LH, Laughlin MR, Rothman DL, Shulman RG. ^{13}C NMR relaxation times of hepatic glycogen in vitro and in vivo. Biochemistry 1990;29: 6815–6820.
30. Overloop K, Vanstapel F, Vanhecke P. C13 NMR relaxation in glycogen. Magn Reson Med 1996;36:45–51.
31. Posse S, Schuknecht B, Smith ME, van Zijl PC, Herschkowitz N, Moonen CT. Short echo time proton MR spectroscopic imaging. J Comput Assist Tomogr 1993;17:1–14.
32. Saner M, McKinnon G, Boesiger P. Glycogen detection by in vivo ^{13}C NMR: a comparison of proton decoupling and polarization transfer. Magn Reson Med 1992;28:65–73.
33. Sibson NR, Dhankhar A, Mason GF, Rothman DL, Behar KL, Shulman RG. Stoichiometric coupling of brain glucose metabolism and glutamatergic neuronal activity. Proc Natl Acad Sci USA 1998;95: 316–321.
34. Sonnewald U, Gribbestad IS, Westergaard N, Nilsen G, Unsgard G, Schousboe A, Petersen. Nuclear magnetic resonance spectroscopy: biochemical evaluation of brain function in vivo and in vitro. Neurotoxicology 1994;15:579–590.
35. Malloy C, Sherry A, Jeffrey F. Analysis of tricarboxylic acid cycle of the heart using ^{13}C isotope isomers. Am J Physiol 1990;259:H987–995.
36. Pfeuffer J, Tkac I, Provencher SW, Gruetter R. Toward an in vivo neurochemical profile: quantification of 18 metabolites in short-echo-time ^{1}H NMR spectra of the rat brain. J Magn Reson 1999;141:104–120.
37. Trabesinger AH, Weber OM, Duc CO, Boesiger P. Detection of glutathione in the human brain in vivo by means of double quantum coherence filtering. Magn Reson Med 1999;42:283–289.
38. Pfeuffer J, Tkac I, Choi I-Y, Merkle H, Ugurbil K, Garwood M, Gruetter R. Localized in vivo 1H NMR detection of neurotransmitter labeling in rat brain during infusion of [1-^{13}C] D-glucose. Magn Reson Med 1999; 41:1077–1083.
39. Barany M, Arus C, Chang YC. Natural-abundance ^{13}C NMR of brain. Magn Reson Med 1985;2:289–295.
40. Willker W, Engelmann J, Brand A, Leibfritz D. Metabolite identification in cell extracts and culture media by proton-detected 2D-H,C-NMR spectroscopy. J MR Anal 1996;2:21–32.